Perturbation of Nanoplastics on Biomembranes: Molecular Insights from Neutron Scattering

*Shuo Qian*1, Honghai Zhang 1, Wellington Leite 1, Andrew E. Whitten 2, Piotr Zolnierczuk 1, Qiu Zhang 1*

1 Oak Ridge National Laboratory, Oak Ridge, TN USA

2 Australian Nuclear Science and Technology Organisation, Lucas Heights, NSW 2234, Australia

* Corresponding Author

Shuo Qian, Oak Ridge National Laboratory, Oak Ridge, TN

qians@ornl.gov

865-241-1934

This manuscript has been authored by UT-Battelle, LLC, under contract DE-AC05-00OR22725 with the US Department of Energy (DOE). The US government retains and the publisher, by accepting the article for publication, acknowledges that the US government retains a nonexclusive, paid-up, irrevocable, worldwide license to publish or reproduce the published form of this manuscript, or allow others to do so, for US government purposes. DOE will provide public access to these results of federally sponsored research in accordance with the DOE Public Access Plan (https://www.energy.gov/doe-public-access-plan).

https://doi.org/10.26434/chemrxiv-2024-mwgqf **ORCID:** https://orcid.org/0000-0002-4842-828X Content not peer-reviewed by ChemRxiv. **License:** CC BY-NC-ND 4.0

ABSTRACT

Plastic waste is now pervasive in the environment, breaking down into microplastics and nanoplastics under many environmental conditions. These particles have been found in various ecosystems and even in human tissues, raising significant environmental and health concerns. In this study, we investigated the interaction of polystyrene nanoplastics, with and without surface modifications, on biomembrane structures using contrast-matching small-angle neutron scattering and neutron spin echo spectroscopy. The neutron contrast matching enabled selective study of biomembranes in the presence of nanoplastics. Two model membranes were employed: a simple zwitterionic bilayer (i.e., dimyristoylphosphatidylcholine [DMPC]) and an *Escherichia coli* lipid extract as a bacterial membrane model. The results show profound membrane disruptions, including thinning, vesicle fragmentation, lipid monolayer formation, and inter-vesicle aggregation, with the most severe effects observed in DMPC membranes. Notably, *E. coli* membranes exhibited greater resilience, suggesting that biological membranes with diverse lipid compositions may mitigate some nanoplastic particle–induced damage. These findings highlight the potential risks posed by environmental nanoplastic particles to biological membranes, with insights for molecular-level interactions and the environmental toxicity of nanoplastics. This work provides a foundation for future studies into nanoplastic–biomembrane interactions and their broader implications for health and environment.

https://doi.org/10.26434/chemrxiv-2024-mwgqr **ORCID:** https://orcid.org/0000-0002-4842-828X Content not peer-reviewed by ChemRxiv. **License:** CC BY-NC-ND 4.0

KEYWORDS: Nanoplastics, nanoparticle, lipid membrane, *E. coli*, contrast matching, SANS, NSE.

SYNOPSIS: The effect of nanoplastics on biomembranes is not well understood. This study highlights the complex interplay between nanoplastics and biomembranes and underscores the need to fully assess the biological risks of nanoplastics.

TOC

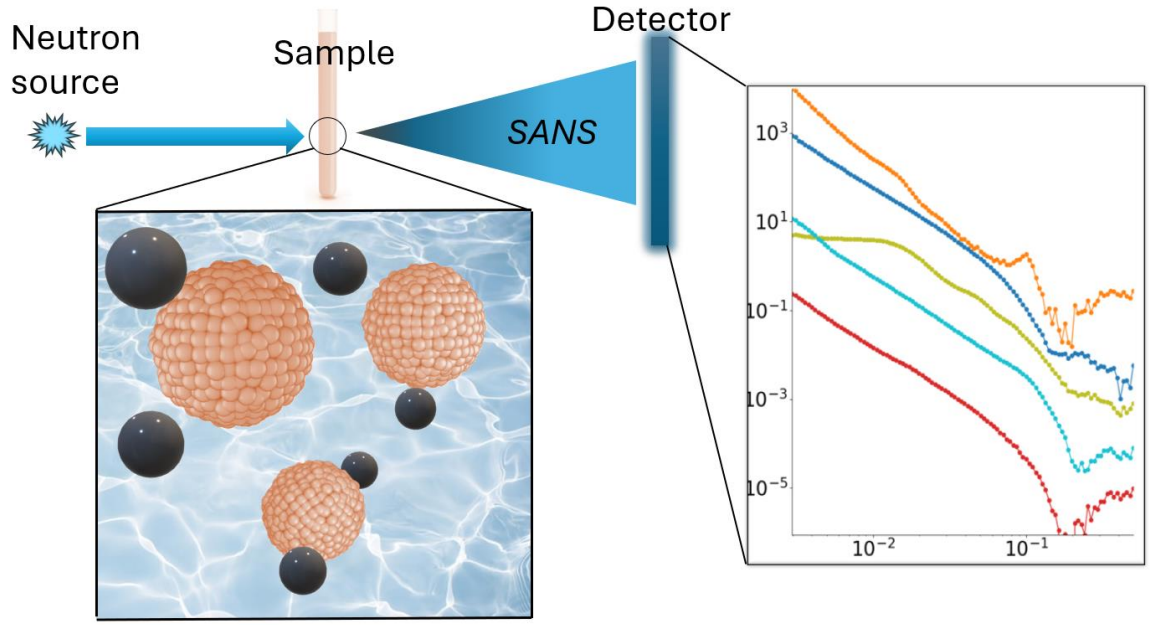

https://doi.org/10.26434/chemrxiv-2024-mwgqr **ORCID:** https://orcid.org/0000-0002-4842-828X Content not peer-reviewed by ChemRxiv. **License:** CC BY-NC-ND 4.0

1. INTRODUCTION

Plastic waste is now ubiquitous in the environment. Under environmental factors such as moderate temperature, solar radiation, oxidative conditions, and many others, plastic waste is being reduced to small particles [1,2]. The transformation of plastic items into finer plastic particles, including so-called microplastics and nanoplastics is now recognized as a continuous process in the environment. Recent studies demonstrate that even supposedly stable plastics can degrade into fine particles under common environmental conditions [3–5]. They have been shown to affect all kingdoms of life, both directly and indirectly; the most significant harm has been observed in marine environments [6].

Recent studies highlight the pervasive nature of microplastics and nanoplastics: they have been found in various ecosystems and even in human tissues. For instance, researchers have detected nanoplastics in human placentas, raising concerns about potential influence on fetal development [7]. Additionally, nanoplastics have been observed crossing the blood–brain barrier in animal models, suggesting possible neurological effects [8]. Nanoplastics promote in vitro aggregation of α-synuclein, which is associated with dementias such as Parkinson's disease [9]. In vitro studies have shown that micro- and nanosized plastic particles can accumulate in the tissues of various living organisms, including mussels, shrimp, and fish [10–12]. These results all point to the presence of plastic particles in biosphere as a potentially significant environmental and health issue, motivating the urgent need to understand the interaction of plastic particles at different biological levels [13].

In this study, we focus on how nanoplastic particles (NPs) with different surface modifications interact and modify biomembrane molecular structures under various conditions using contrast-

https://doi.org/10.26434/chemrxiv-2024-mwgqr **ORCID:** https://orcid.org/0000-0002-4842-828X Content not peer-reviewed by ChemRxiv. **License:** CC BY-NC-ND 4.0

matching small-angle neutron scattering (SANS), along with additional insights into membrane dynamics from neutron spin echo (NSE) spectroscopy. NPs have been found to have a greater potential for accumulation and translocation within host tissues [11,14,15] than their micro-sized counterpart. Many studies to date show that particle size is a primary factor for plastic particles in entering and distributing within tissues and cells. The significantly increased surface area of smaller plastic particles can also adsorb and transport organic pollutants [16], transforming them into vehicles for toxic substances within host organisms. They can act as Trojan horses, facilitating the uptake of other environmental contaminants such as heavy metals and persistent organic pollutants [17–20]. Biomembranes are important semipermeable barriers that separate cells or organelles from their surrounding environment and are crucial interfaces for many biological processes. Recent evidence suggests that plastic particles can enter cells via various pathways, including endocytosis and direct membrane penetration [21–25]. Some studies have also shown the destabilizing effect on lipid membranes [26–31]; however, direct experimental insights into how NPs alter membrane structure during their interaction are currently lacking.

SANS is a bulk technique capable of providing hierarchical structure information across different length scales from a few nanometers to a few hundred nanometers simultaneously. It is a key method for probing from trans-bilayer membrane structure to overall vesicle morphology in solutions [32–37]. The different sensitivity of neutrons to hydrogen and deuterium allows varying contrast between solute and solvent by changing D_2O/H_2O ratios of the latter [38,39]. The contrast matching with this isotopic sensitivity enabled selective observation of membrane structure by eliminating the scattering from NPs. NSE spectroscopy reveals sub-microsecond dynamic motions on length scales from a few to hundreds of nanometers, allowing the derivation of various elastic-mechanical properties, such as membrane bending modulus and bilayer area

https://doi.org/10.26434/chemrxiv-2024-mwgqr **ORCID:** https://orcid.org/0000-0002-4842-828X Content not peer-reviewed by ChemRxiv. **License:** CC BY-NC-ND 4.0

compressibility, to corroborate the structure changes [40–42]. Two model membrane systems were selected for this study: 1,2-dimyristoyl-sn-glycero-3-phosphocholine (DMPC) as a simple zwitterionic model bilayer, and *Escherichia coli* (*E. coli*) total lipid extract as a model for bacterial membranes that are ubiquitous in the environment. Notably, fully deuterated *E. coli* cells were grown, and their total lipid was extracted and used to enhance neutron contrast. Spherical polystyrene (PS) NPs with well-defined and uniform size were selected as a model particle. They are either unmodified or surface modified such as aminated PS (AM) (positively charged) and carboxylated PS (CM) (negatively charged). Although this model system may not fully capture the heterogeneity of environmental NPs, their well-defined size and properties have enabled recent research to provide valuable insights into the environmental impact of NPs [9,14,15,27].

2. MATERIALS AND METHODS

2.1. Nanoplastics and Lipids

PS latex particles, including unmodified PS and surface-modified AM and CM, were purchased from Magsphere Inc (Pasadena, California). The diameters are 38 nm for PS (Lot No. PS3455A-620), 43 nm for CM (Lot No. CM3160C), and 53 nm for AM (Lot No. AM4818A). The stocks were in aqueous suspension at a concentration of 10% w/v. Chain per-deuterated DMPC (D54-DMPC) and regular protiated DMPC were purchased from Avanti Lipids (Birmingham, Alabama). They were used as delivered.

To produce *E. coli* total lipid, *E.coli* BL21 (DE3) strain was inoculated into 5 mL of Luria–Bertani media from glycerol stock and incubated at 37 °C overnight. The cell cultures were then adapted to grow in D_2O Enfors-based minimal media with D-glycerol as the carbon source. The cells

https://doi.org/10.26434/chemrxiv-2024-mwgqr **ORCID:** https://orcid.org/0000-0002-4842-828X Content not peer-reviewed by ChemRxiv. **License:** CC BY-NC-ND 4.0

underwent three exchanges of media to ensure complete adaption from H_2O to D_2O-based media. Then the culture was grown at 37 °C overnight in the D_2O Enfors minimal media [43] supplemented with D-glycerol with initial inoculation at an optical density at 600 nm of approximately 0.1. The cells were harvested by centrifugation at 6000× *g* for 30 min and then washed with 1% NaCl three times followed by freeze-drying for 48 h before lipid extraction. The *E. coli* total lipid was extracted using the modified Bligh and Dyer method [44]. In brief, 250 mL chloroform, 500 mL methanol, and 200 mL water were sequentially added to the freeze-dried cells (1.1 g) to achieve a final chloroform:methanol:water ratio of 1:2:0.8 (v/v/v). The cells were vortexed for 15 s immediately following the addition of each solvent and allowed to stand for approximately 18 h at room temperature with stirring. This process was followed by the addition of chloroform (250 mL) and water (250 mL) to obtain a final chloroform:methanol:water ratio of 1:1:0.9 (v/v/v) to separate the aqueous and organic fractions of the mixture. A separatory funnel was used to collect the lower chloroform phase, which contains the lipid extract. The chloroform–methanol mixture was then evaporated under reduced pressure using a rotovap (Buchi, R-205). The lipid extract was dried under vacuum overnight.

2.2. Large Unilamellar Vesicle Preparation

The large unilamellar vesicles (LUVs) were prepared following the method established previously [37,45]. Briefly, D54-DMPC or *E. coli* lipid was dispersed in 26% v/v D_2O to obtain 15 mg/mL stock solution. After extensive vortexing, the solutions underwent at least three freeze-thaw cycles by alternately placing them on a hot plate at 30 °C and in a freezer at −80 °C. The LUVs were made using an Avanti mini-extruder (Alabaster, Alabama), with membranes of 0.1 μm diameter pores. The solution was extruded for 21 passes for the final LUV solutions. Different PS suspensions were titrated into the final LUV solutions to achieve different particle

https://doi.org/10.26434/chemrxiv-2024-mwgqr **ORCID:** https://orcid.org/0000-0002-4842-828X Content not peer-reviewed by ChemRxiv. **License:** CC BY-NC-ND 4.0

concentrations of 0.5%, 1%, and 2% w/v. The samples were stored at 4 °C for up to one week if not immediately measured.

2.3. SANS Experiment

The SANS measurements were performed using the BIO-SANS instrument at the High Flux Isotope Reactor and the EQ-SANS instrument at the Spallation Neutron Source (SNS), both US Department of Energy (DOE) Office of Science user facilities at Oak Ridge National Laboratory (ORNL) [46], and the Bilby instrument at the Australian Nuclear Science and Technology Organisation's OPAL reactor [47]. The lipid solutions were transferred into quartz circular cells with a 1 mm beam path (Hellma, Germany) for measurements. The samples were kept at 30 °C, and instruments were set to a Q range covering 0.003 to 0.5 $Å^{-1}$. The acquired data were subsequently processed using the facility-provided data reduction software, resulting in 1D scattering curves (I vs. Q) presented in absolute scale, where I is the scattering intensity arising from the contrast between the lipids and the solvent, and Q is the scattering vector from $Q = 4\pi\sin\theta/\lambda$, where θ is half of the scattering angle, and λ is the neutron wavelength.

2.4. SANS Data Analysis

To determine the contrast matching point (CMP) of PS NPs, the scattering intensity I was measured at different D_2O ratios (v/v). From a linear regression of $\sqrt{I}$ vs. D_2O ratio (v/v), the CMP, in terms of D_2O ratio, was determined as the line intercepts the zero intensity [38].

The data fitting was performed in SASView software (sasview.org). According to the scattering profiles and different Q ranges corresponding to their length scales, various fittings can be performed to extract structural information. The overall power law decay of intensity is

https://doi.org/10.26434/chemrxiv-2024-mwgqr ORCID: https://orcid.org/0000-0002-4842-828X Content not peer-reviewed by ChemRxiv. License: CC BY-NC-ND 4.0

described by $I(Q)$ = scale × q^{-p} + background, where the exponent factor p provides a dimensional description of the scattering object.

The trans-bilayer membrane structure, dominated by the hydrocarbon chain high in deuterium, was modeled as a single slab of neutron scattering length density. It was fitted with an isotropic lamellar model. The scattering intensity $I(Q)$ for the randomly oriented bilayer in a vesicle is $I(Q)$ = scale × $(2\pi P(Q)/Q^2 d)$ + background, where the form factor is $P(Q) = (2\Delta\rho^2/Q^2) \times (1 - \cos(Qd))$. The total layer thickness is given by d, and $\Delta\rho$ is the scattering length density difference (the contrast) between the lipid and the solvent [48]. The polydispersity of the thickness d is assumed to be a Gaussian distribution implemented in SASView. In the case of inter-bilayer peak presented in the data, a Caillè structure factor is used as implemented in SASView to determine the d-spacing.

A generalized Guinier–Porod function is used to fit low-Q data when applicable. This empirical model provides the size and dimensionality of the sample, including shape intermediates between typical well-defined 1D, 2D, or 3D shapes (e.g., long rod, thin/extended sheet, or globular particle, respectively) [49]. In the case of a possible globular 3D shape within the Q range, the Guinier function is used to obtain the radius of gyration R_g by fitting $I(Q)$ = scale × $\exp\{(-Q^2 R_g^2/3)\}$ + background [50].

2.5. NSE Experiment and Data Analysis

NSE experiments were performed at the SNS NSE instrument (BL-15) at ORNL [51]. Three different NPs were titrated to the protiated DMPC LUVs in D_2O to 1% concentration. The samples were measured at 30 °C with a precision of ±0.5 °C. Two neutron wavelength bands of 5–8 Å and 8–11 Å were chosen to cover Fourier times from about 0.07 to 100 ns and a Q range of

https://doi.org/10.26434/chemrxiv-2024-mwgqr ORCID: https://orcid.org/0000-0002-4842-828X Content not peer-reviewed by ChemRxiv. License: CC BY-NC-ND 4.0

about 0.055–0.10 $Å^{-1}$. Background was subtracted from D_2O samples with the same sample cell size. Data reduction was performed using the DrSPINE program [52].

The data analysis follows Zilman and Granek [53], using a freestanding single-membrane fluctuation model to fit the intermediate scattering function $\frac{S(Q,t)}{S(Q,0)} = e^{-(\Gamma(Q)\,t)^{\frac{2}{3}}}$, where Q and t are the wavenumber transfer and the Fourier time, respectively. Then the Q-dependent relaxation rate was obtained from the fitting $\Gamma(Q)$. The effective bending modulus $\tilde{\kappa}$ can be obtained by the equation from Watson and Brown [54]: $\Gamma(\mathrm{Q}) = 0.025\,\gamma\sqrt{\frac{k_BT}{\tilde{\kappa}}}\frac{k_BT}{\eta_{D_2O}}Q^3$, where γ is assumed to be 1 when $\tilde{\kappa} \gg k_BT$, which is typical for lipid bilayers near room temperature [53,55], and η_{D_2O} is the viscosity of D_2O at 30 °C.

3. RESULTS AND DISCUSSION

3.1. Effects on DMPC LUV

First, from the contrast variation series measured at different D_2O ratios, we determined that the CMP for PS NPs is 26% D_2O (Fig. 1). Therefore, all the samples with LUV were prepared in 26% D_2O to eliminate the scattering from PS NPs and highlight deuterated lipids D54-DMPC and *E. coli* lipid with CMP of approximately 95% D_2O (D54 chain) and approximately 101.7% D_2O-equivalent [56], respectively.

https://doi.org/10.26434/chemrxiv-2024-mwgqr **ORCID:** https://orcid.org/0000-0002-4842-828X Content not peer-reviewed by ChemRxiv. **License:** CC BY-NC-ND 4.0

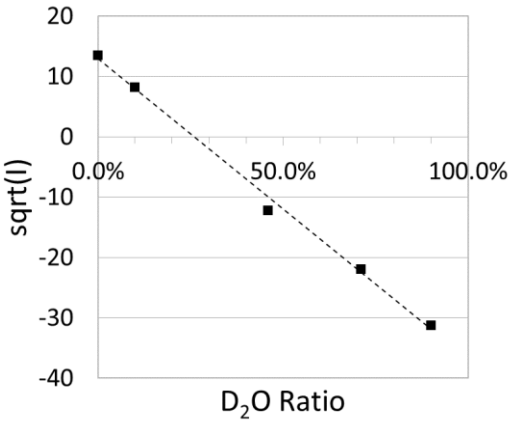

Figure 1. Contrast match point of the PS nanoparticle. The inception of the linear fitting of the data points to the zero-intensity line indicates that the PS CMP is 26% D_2O.

DMPC is a zwitterionic lipid with relatively flat intrinsic curvature. It is widely used to form unilamellar vesicles as a simple model membrane system[32,36]. The SANS data covers a large span of length scales including an overall morphology of the LUVs (low Q, ~< 0.01 $Å^{-1}$), a large expanse of bilayer thin sheet (medium Q range ~0.01 to ~0.04 $Å^{-1}$) and a trans-bilayer structure (high Q, ~> 0.04 $Å^{-1}$); the length scale in the real space relates to the reciprocal space Q by $2\pi/Q$. For almost all DMPC samples, the low-Q scattering intensity exhibits generally the same slope as in the medium Q range (Fig. 2, as shown parallel to the dash line). The slope can be obtained as a power law exponent of about 2, consistent with a thin 2D sheet structure and typical of LUV lipid bilayer.

https://doi.org/10.26434/chemrxiv-2024-mwgqr **ORCID:** https://orcid.org/0000-0002-4842-828X Content not peer-reviewed by ChemRxiv. **License:** CC BY-NC-ND 4.0

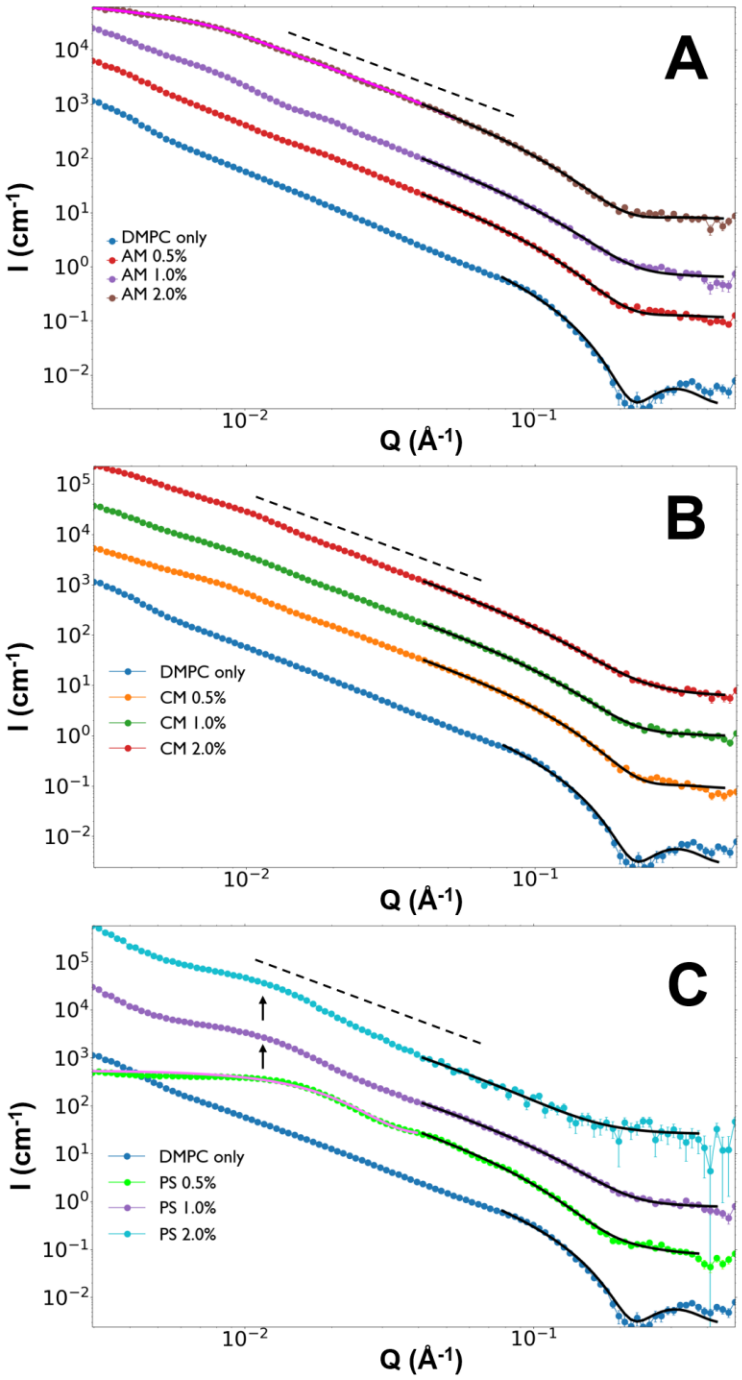

Figure 2. Scattering profiles D54-DMPC ULV with different PS NPs concentrations (A) AM (B) CM (C) PS. The dash line indicates the power law exponent of 2. The low-*Q* fitting, if any, is overlaid on the data with a magenta line. The high Q fitting is overlaid with a black line. The profiles are offset by a scale factor of 10 for clarity.

https://doi.org/10.26434/chemrxiv-2024-mwgqr **ORCID:** https://orcid.org/0000-0002-4842-828X Content not peer-reviewed by ChemRxiv. **License:** CC BY-NC-ND 4.0

The high-Q region shows the more detailed structure across the lipid bilayer. The DMPC-only scattering profile displays a sharp minimum near $Q = 0.2$ Å^{-1}, indicating a well-defined bilayer–water interface and a slab-like deuterated hydrocarbon chain within the bilayer. Upon addition of NPs, all minima are reduced to blunt kinks, suggesting increased bilayer thickness polydispersity. The much shallower slope approaching the kinks further shows the bilayer–water interface is blurrier because the Porod exponent deviates to much less than 4 [57].

The effect of the different NP types and concentrations overall vesicle morphology also varies. For AM, at a very high concentration (2%), the scattering curve starts to flatten at low Q, suggesting the formation of particles smaller than the original LUVs, possibly smaller vesicles (Fig. 2A). Fitting these data with the Guinier–Porod function yields an R_g of approximately 148 Å, much smaller than the extruded LUV radius of about 500 Å. Both sizes likely coexist. By contrast, the Porod exponent is close to 2, indicating that the large bilayer thin sheet remains present. The high-Q data (>0.04 Å^{-1}) were further fitted by the lamellar model for the trans-bilayer structure. The DMPC-only sample shows a thickness of 27.6 ± 0.1 Å without the thickness polydispersity (Table 1). Adding AM significantly reduces the bilayer thickness and significantly increases the thickness polydispersity (Fig. 3A). For example, 0.5% of AM thins the bilayer to 24.6 ± 0.2 Å with about 19% polydispersity. Then 1% AM further thins the bilayer and increases polydispersity. The trend partially reverses at 2% AM with slightly increased thickness and decreased polydispersity then at 1% AM, coincident with the possible formation of smaller vesicles. If the thinning effect is caused by the stretching of membrane in the presence of AM NPs [26,58], then the reduction may indicate that the tension caused by AM particles is partially relieved as smaller vesicles start to form (Fig. 3B).

https://doi.org/10.26434/chemrxiv-2024-mwgqr **ORCID:** https://orcid.org/0000-0002-4842-828X Content not peer-reviewed by ChemRxiv. **License:** CC BY-NC-ND 4.0

Table 1. Lamellar fitting results for DMPC samples

	Thickness (Å)	Thickness polydispersity (%)	Note
DMPC lipid only	27.6 ± 0.1	Not used	
AM 0.5%	24.6 ± 0.2	19.9 ± 1.7	
AM 1%	21.6 ± 0.6	30.3 ± 4.8	
AM 2%	24.7 ± 0.3	15.2 ± 4.0	Low Q is fitted with the Guinier–Porod function
CA 0.5%	24.0 ± 0.1	19.7 ± 1.3	
CA 1%	22.4 ± 0.3	28.5 ± 2.7	
CA 2%	18.3 ± 1.1	51.5 ± 8.2	
PS 0.5%	28.6 ± 0.2	31.7 ± 1.3	Low Q is fitted with the Guinier function
PS 1%	21.7 ± 0.6	33.6 ± 4.6	
PS 2%	14.8 ± 1.6	75.5 ± 13.5	

https://doi.org/10.26434/chemrxiv-2024-mwgqr **ORCID:** https://orcid.org/0000-0002-4842-828X Content not peer-reviewed by ChemRxiv. **License:** CC BY-NC-ND 4.0

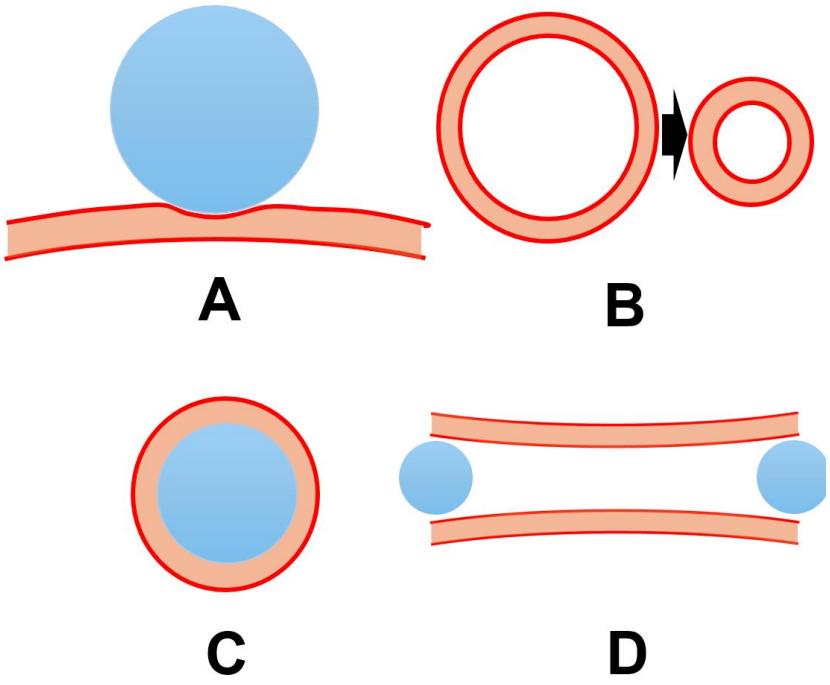

Figure 3. Schematic representation of the structure changes caused by NPs revealed by SANS. (A) Membrane thinning, (B) smaller vesicle formation, (C) lipid monolayer around PS NPs, and (D) inter-vesicle aggregation. The blue circle represents NP, the red line profile is the lipid headgroup, and the orange is the lipid chain.

CM also induces thickness changes, although less drastically than AM. As shown in Fig. 2B, the power law exponents are the same as the DMPC sample at all concentrations. Smaller vesicles do not form. The lamellar model fitting results show a general decreasing bilayer thickness and increasing polydispersity as the CM concentration increases (Fig. 3A). The thickness changes to 18.3 ± 1.1 Å, and polydispersity is greater than 50%, indicating a significant disturbance of CM on the membrane.

Unmodified PS NPs exhibited the most significant change (Fig. 2C). At only 0.5% concentration, much smaller particles are formed, as indicated by the leveling scattering profile

https://doi.org/10.26434/chemrxiv-2024-mwgqr **ORCID:** https://orcid.org/0000-0002-4842-828X Content not peer-reviewed by ChemRxiv. **License:** CC BY-NC-ND 4.0

at low Q. This can be fitted with the Guinier function. The result indicates the R_g of the smaller particles is about 100 Å. Then, at higher concentrations of 1% and 2%, the scattering profiles revert to a power law decay with exponent of about 2. However, the identical undulation near 0.01 $Å^{-1}$ (highlighted by arrows in Fig. 2C) from both samples indicates a mixture of smaller particles like the ones presented in the 0.5% PS sample. Fitting at the high-Q region reveals a significant decrease in lamellar thickness at 1% and 2% PS. The thickness at 2% PS is almost halved compared with the DMPC-only sample, accompanied by greatly increased polydispersity to more than 75%. This result suggests great disruption of bilayer by the PS NPs to form monolayer, likely on the surface of hydrophobic PS NPs (Fig. 3C) [30]. Given the large polydispersity, LUVs and smaller PS-monolayer particles likely coexist in the sample. However, fitting with the Guinier function for accurate particle sizes combined with the power law cannot yield a satisfactory result, indicating a more complex mixture of different structures in the sample. Overall, large thin sheets remain, as the power law exponent of 2 suggests, but some of the sheets are monolayer instead of bilayer. This significant effect can also be seen from NSE results (Fig. 4). Adding 1% AM or CM to the DMPC change the effective bending modulus of DMPC bilayer about 20% to 30%, either making the bilayer more rigid or softer, respectively. However, a large decrease in membrane rigidity happens with 1% PS NPs. The effective bending changes from 203 ± 8 k_BT to 24 ± 2 k_BT, almost an order of magnitude smaller. This result suggests some fundamental changes to the membrane, corroborating the formation of monolayer indicated by the thickness reduction. The intrinsic bending modulus and the bilayer area compressibility modulus can be derived from the effective bending modulus; however, they are based on models of lipid bilayer rather than monolayer. They are presented in the Supporting Information.

https://doi.org/10.26434/chemrxiv-2024-mwgqr **ORCID:** https://orcid.org/0000-0002-4842-828X Content not peer-reviewed by ChemRxiv. **License:** CC BY-NC-ND 4.0

The greater change is likely driven by the hydrophobic nature of PS, which favors interaction with the hydrophobic core of the bilayer. The effects of PS NPs, even at low concentrations, raise concerns about their potential influence on biological membranes. Although the charged and hydrophilic nature of AM and CA NPs appears to ease some of these effects compared with the unmodified PS NPs, the observed structural perturbations such as membrane thinning (Fig. 3A) and smaller vesicle formation (Fig. 3B) are still concerning.

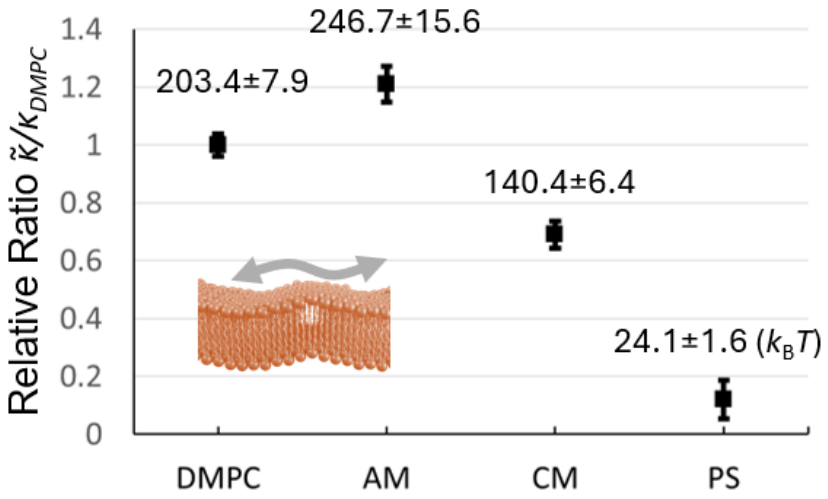

Figure 4. Relative ratios of the effective bending moduli $\tilde{\kappa}$ to the DMPC-only sample. The $\tilde{\kappa}$ values in units of k_BT were labeled next to the markers. The inset cartoon illustrates the membrane bending measured from NSE.

3.2. Effect on *E. coli* lipid membrane

The deuterated *E. coli* lipid, extracted from cells grown in deuterated media, provides a more environmentally relevant model membrane system compared with single-component lipid vesicles. Its complex composition of lipids with varying chain lengths and headgroups

https://doi.org/10.26434/chemrxiv-2024-mwgqr ORCID: https://orcid.org/0000-0002-4842-828X Content not peer-reviewed by ChemRxiv. License: CC BY-NC-ND 4.0

(predominantly negatively charged Phosphatidylglycerol (PG) and highly intrinsically curved Phosphatidylethanolamine (PE), with minor components such as Phosphatidic acids, Phosphatidylserine, and Lyso-PE) reflects the diverse lipid makeup of bacterial membranes. The ubiquitous distribution of bacteria in the environment offers abundant opportunities for NP interaction with such membranes. The contrast-matching point of the *E. coli* lipid was determined to be about 101.7% D_2O-equivalent, standing out prominently in 26% D_2O used for contrast matching PS.

The LUVs formed from *E. coli* lipid also exhibit a well-defined unilamellar bilayer, as evidenced by the low-*Q* data indicating an extended bilayer thin sheet structure (Fig. 5). In contrast to the DMPC bilayer, the first minimum between 0.1 and 0.2 $Å^{-1}$ is less prominent, indicating some degree of thickness polydispersity originated from its complex composition with lipids of different chain length. Fitting this region, the lamellar model shows a much thicker bilayer of 41.2 Å with about 17.5% ± 0.8% thickness polydispersity (Table 2). This result is consistent with its higher degree of deuteration, including the headgroups and the presence of both long-chain and short-chain lipids [56]. Interestingly, the addition of NPs led to sharper minima around the region, suggesting a decrease in thickness polydispersity; therefore, the interaction yields a more rigid and uniform membrane as NPs round up different lipids. At the same time, the addition of NPs reduces the bilayer thickness for all the samples, as evidenced by the shifts in the positions of the first minima to higher *Q* values. This effect was observed even at the lowest NP concentrations tested, demonstrating the significant influence of both unmodified and surface-modified NPs.

https://doi.org/10.26434/chemrxiv-2024-mwgqr **ORCID:** https://orcid.org/0000-0002-4842-828X Content not peer-reviewed by ChemRxiv. **License:** CC BY-NC-ND 4.0

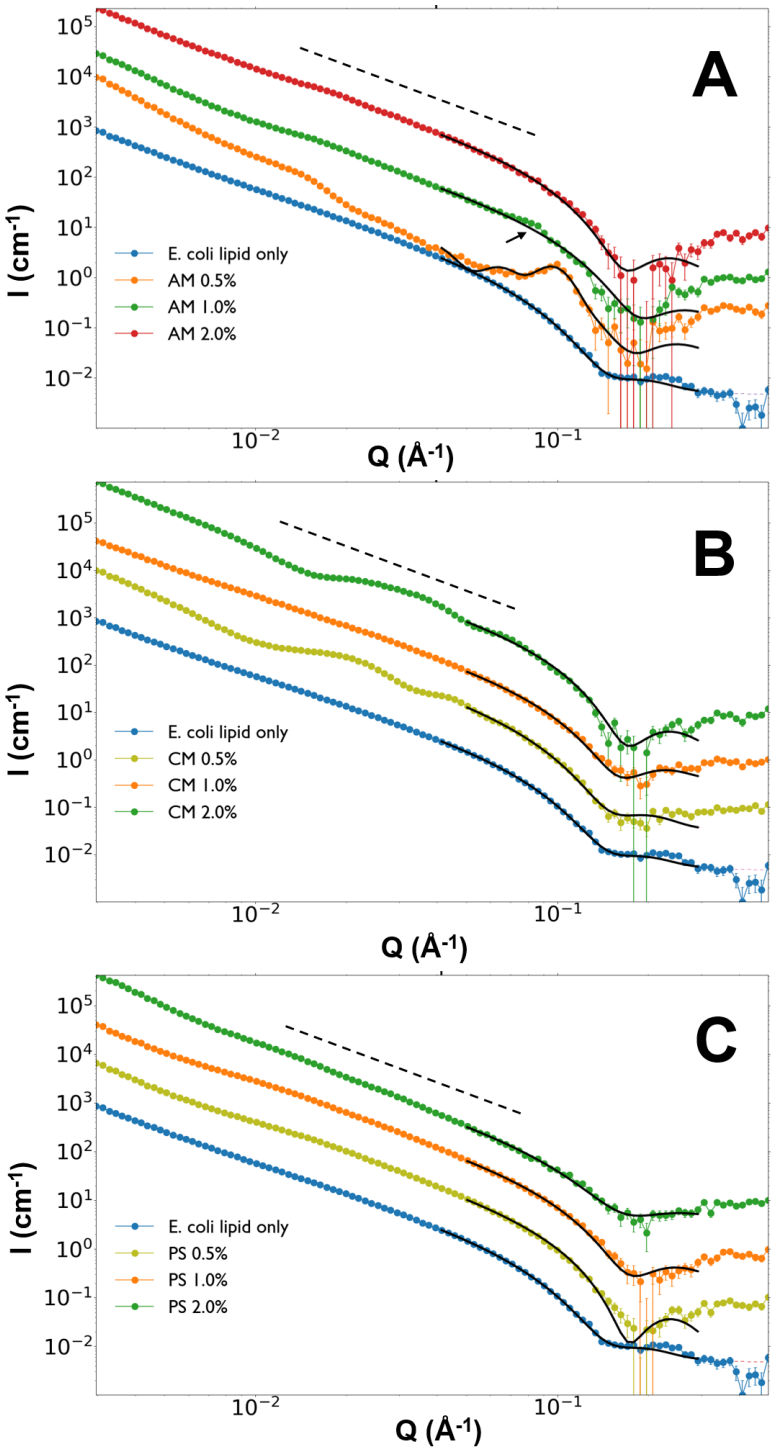

Figure 5. Scattering profiles of *E. coli* lipid ULV with different PS NP concentrations for (A) AM, (B) CM, and (C) PS. The dashed line indicates the power law exponent of 2. The high-Q fitting is overlaid with a black line. The profiles are offset by a scale factor of 10 for clarity.

https://doi.org/10.26434/chemrxiv-2024-mwgqr **ORCID:** https://orcid.org/0000-0002-4842-828X Content not peer-reviewed by ChemRxiv. **License:** CC BY-NC-ND 4.0

Table 2. Lamellar fitting results for *E. coli* lipid samples

	Thickness (Å)	Thickness polydispersity (%)	Note
E. coli lipid only	41.2 ± 0.1	17.6 ± 0.8	
AM 0.5%	34.4 ± 0.8	Not used	Caillè structure factor is used to combine with lamellar form factor
AM 1%	32.5 ± 0.3	Not used	
AM 2%	36.6 ± 0.3	Not used	
CA 0.5%	40.8 ± 0.2	15.9 ± 1.1	
CA 1%	37.5 ± 0.2	Not used	
CA 2%	36.4 ± 0.2	Not used	
PS 0.5%	36.2 ± 0.2	Not used	
PS 1%	34.9 ± 0.2	Not used	
PS 2%	33.9 ± 0.5	Not used	

The lamellar model fitting results also substantiate this thinning effect. For example, adding AM reduces the bilayer thickness from 41.2 Å to between about 32 and 37 Å, with no polydispersity needed to fit the data well. Adding CM and PS NPs reduces the bilayer thickness gradually in a concentration dependent manner. No halved reduction in the thickness occurs for any of the samples, unlike in some of DMPC samples. This result indicates that the bilayer structure is preserved, with no evidence of monolayer formation.

Although most NP additions preserve the unilamellar structure, the addition of 0.5% AM induces inter-vesicle attraction, evidenced by a prominent peak at $Q = 0.1$ Å^{-1} (corresponding to a repeating spacing of 60.0 Å fitted by Caillè structure factor). This is possible for positively charged AM NPs

https://doi.org/10.26434/chemrxiv-2024-mwgqr **ORCID:** https://orcid.org/0000-0002-4842-828X Content not peer-reviewed by ChemRxiv. **License:** CC BY-NC-ND 4.0

to bring negatively charged *E. coli* bilayer in close proximity (Fig. 3D). Even in the 1% AM sample, a small shoulder peak can be seen near Q = 0.08 Å^{-1} on top of the lamellar form factor (indicated by the arrow in Fig. 5A). However, increasing AM concentration may balance out the overall charge distribution around the LUVs, so the inter-vesicle aggregation is greatly reduced in the 1% AM sample and eventually disappears in the 2% AM sample.

At low and medium Q, the changes in *E. coli* lipid bilayer are also less drastic than in DMPC. The extended thin sheet with power law exponent of 2 occurs in all the samples. No smaller particles form, even in the most hydrophobic PS NPs, unlike DMPC.

The complex lipid composition of the *E. coli* membrane, including charged lipids such as PG and lipids with high intrinsic curvature such as PE, as well as the diversity in chain lengths and saturation, appears to partially mitigate the influence of NPs compared with the simpler DMPC system. However, the membrane thinning in all samples even at low NP concentrations, and inter-vesicle aggregation in some cases, significantly affect the membranes.

3.3.Implications

This study employed well-defined spherical PS particles. Unmodified, these particles are highly hydrophobic and quite rigid. Upon surface modification with amine groups, the particles become more hydrophilic and positively charged, which facilitates interactions with negatively charged bacterial membranes. Conversely, carboxylated modifications render the particles more hydrophilic while imparting a negative charge, causing repulsion from bacterial membranes. At low volume fractions, these particles also exert osmotic pressure in solution [59]. The particle diameters, around 40–50 nm, fall on the relatively small end of NPs typically found in environmental contexts. As a model, they can be found at tissue levels and can interact with

https://doi.org/10.26434/chemrxiv-2024-mwgqr **ORCID:** https://orcid.org/0000-0002-4842-828X Content not peer-reviewed by ChemRxiv. **License:** CC BY-NC-ND 4.0

membrane-associated proteins such as α-synuclein [9,24]. Thus, they serve as well-controlled model NPs for understanding membrane interactions.

The membrane systems employed include a basic phospholipid system and a more complex, biologically relevant membrane, enabling comparison of PS NP interactions under different conditions. The data reveal significant disturbances in both membrane types at the molecular level, regardless of NP concentration, charge, or surface modification. Four primary modes of membrane disruption were identified.

The first, and most prevalent, effect is membrane thinning (Fig. 3A). Although overall vesicle shape remained unchanged, as observed in several DMPC and *E. coli* lipid samples, membrane surface adsorption generated tension that thinned the bilayer considerably [58]. This thinning is likely to affect membrane rigidity, potentially influencing various membrane-associated processes (e.g., membrane raft and membrane proteins). The second mode of disruption is vesicle fragmentation into smaller vesicles. This mode was pronounced at high NP concentrations, particularly in AM-DMPC samples (Fig. 3B). The third mode involves lipid monolayer formation induced by interactions with hydrophobic PS NPs (Fig. 3C). Fragmentation and monolayer formation are both destructive to vesicle and bilayer integrity.

Interestingly, the more biologically relevant *E. coli* lipid membrane exhibited some degree of resilience to these destructive effects, showing fewer signs of damage. This result suggests that membranes composed of a diverse range of lipids—especially with charged lipids and different chain length, as seen in biological systems—may be more resistant to NP-induced damage. Nonetheless, the fourth mode of structural alteration—inter-vesicle aggregation—was noted at

https://doi.org/10.26434/chemrxiv-2024-mwgqr **ORCID:** https://orcid.org/0000-0002-4842-828X Content not peer-reviewed by ChemRxiv. **License:** CC BY-NC-ND 4.0

some low NP concentrations and poses potential risks in biological contexts. For example, organelles and transport vesicles within cells could be similarly affected by such aggregation.

These data underscore the potential for NPs to disrupt the delicate balance of biomembrane functions. The observed structural and dynamic changes may impair membrane rigidity, protein functions, and vesicular transport. Significant biological consequences could occur, raising concerns about the environmental and health risks associated with nanoplastics.

The spherical morphology of the NPs used in this study may underestimate the effects that sharper-edged or irregularly shaped particles might exert on membranes. Additional surface properties could also exacerbate NP–membrane interactions, and these variables merit further exploration. Although a standardized approach to nanoplastic studies in this context has not yet been established, the present work demonstrates the utility of SANS contrast matching and offers key insights into NP–membrane interactions that are not accessible by other structural techniques such as cryo-EM [27]. These findings not only advance the understanding of nanoplastics' potential to cause molecular damage but also lay the groundwork for future investigations into the biological impacts of environmentally relevant NPs at the molecular level.

ASSOCIATED CONTENT

Supporting Information. Additional NSE analysis is presented.

Author Contributions

S. Q. designed the research. All performed the research. The manuscript was written through contributions from all authors. All authors have given approval to the final version of the manuscript.

https://doi.org/10.26434/chemrxiv-2024-mwgqr **ORCID:** https://orcid.org/0000-0002-4842-828X Content not peer-reviewed by ChemRxiv. **License:** CC BY-NC-ND 4.0

Acknowledgment

Neutron scattering experiments on the BIO-SANS instrument and lipid deuteration/extraction were supported by the Center for Structural Molecular Biology funded by DOE Biological and Environmental Research project ERKP291. This research used resources at the High Flux Isotope Reactor (the BIO-SANS instrument) and Spallation Neutron Source (the EQ-SANS instrument for preliminary SANS experiment, the NSE instrument), DOE Office of Science user facilities operated by ORNL. The authors acknowledge the support of ANSTO in providing access to instruments, capabilities and facilities used in this via Proposal 16790.

REFERENCES

[1] B. Gewert, M.M. Plassmann, M. Macleod, Pathways for degradation of plastic polymers floating in the marine environment, Environmental Sciences: Processes and Impacts, 17 (2015) 1513–1521.
[2] E. Dube, G.E. Okuthe, Plastics and Micro/Nano-Plastics (MNPs) in the Environment: Occurrence, Impact, and Toxicity, Int J Environ Res Public Health, 20 (2023) 6667.
[3] C.D. Zangmeister, J.G. Radney, K.D. Benkstein, B. Kalanyan, Common Single-Use Consumer Plastic Products Release Trillions of Sub-100 nm Nanoparticles per Liter into Water during Normal Use, Environ. Sci. Technol., (2022).
[4] J.R. Jambeck, R. Geyer, C. Wilcox, T.R. Siegler, M. Perryman, A. Andrady, R. Narayan, K.L. Law, Plastic waste inputs from land into the ocean, Science, (2015).
[5] Microplastics in drinking-water, (n.d.).
[6] K.L. Law, Plastics in the Marine Environment, Annual Review of Marine Science, 9 (2017) 205–229.
[7] A. Ragusa, A. Svelato, C. Santacroce, P. Catalano, V. Notarstefano, O. Carnevali, F. Papa, M.C.A. Rongioletti, F. Baiocco, S. Draghi, E. D'Amore, D. Rinaldo, M. Matta, E. Giorgini, Plasticenta: First evidence of microplastics in human placenta, Environment International, 146 (2021) 106274.
[8] X. Liu, Y. Zhao, J. Dou, Q. Hou, J. Cheng, X. Jiang, Bioeffects of Inhaled Nanoplastics on Neurons and Alteration of Animal Behaviors through Deposition in the Brain, Nano Lett., 22 (2022) 1091–1099.
[9] Z. Liu, A. Sokratian, A.M. Duda, E. Xu, C. Stanhope, A. Fu, S. Strader, H. Li, Y. Yuan, B.G. Bobay, J. Sipe, K. Bai, I. Lundgaard, N. Liu, B. Hernandez, C. Bowes Rickman, S.E. Miller, A.B. West, Anionic nanoplastic contaminants promote Parkinson's disease–associated α-synuclein aggregation, Science Advances, 9 (2023) eadi8716.
[10] K. Mattsson, M.T. Ekvall, L.A. Hansson, S. Linse, A. Malmendal, T. Cedervall, Altered behavior, physiology, and metabolism in fish exposed to polystyrene nanoparticles, Environmental Science and Technology, 49 (2015) 553–561.

https://doi.org/10.26434/chemrxiv-2024-mwgqr **ORCID:** https://orcid.org/0000-0002-4842-828X Content not peer-reviewed by ChemRxiv. **License:** CC BY-NC-ND 4.0

[11] M.A. Browne, A. Dissanayake, T.S. Galloway, D.M. Lowe, R.C. Thompson, Ingested microscopic plastic translocates to the circulatory system of the mussel, Mytilus edulis (L), Environmental Science and Technology, 42 (2008) 5026–5031.
[12] E. Bergami, E. Bocci, M.L. Vannuccini, M. Monopoli, A. Salvati, K.A. Dawson, I. Corsi, Nano-sized polystyrene affects feeding, behavior and physiology of brine shrimp Artemia franciscana larvae, Ecotoxicology and Environmental Safety, 123 (2016) 18–25.
[13] Getting a grip on microplastics' risks, C&EN Global Enterp, 100 (2022) 20–25.
[14] M. Qu, Y. Qiu, Y. Kong, D. Wang, Amino modification enhances reproductive toxicity of nanopolystyrene on gonad development and reproductive capacity in nematode Caenorhabditis elegans, Environ Pollut, 254 (2019) 112978.
[15] A. Pinsino, E. Bergami, C. Della Torre, M.L. Vannuccini, P. Addis, M. Secci, K.A. Dawson, V. Matranga, I. Corsi, Amino-modified polystyrene nanoparticles affect signalling pathways of the sea urchin (Paracentrotus lividus) embryos, Nanotoxicology, 11 (2017) 201–209.
[16] I. Velzeboer, C.J.A.F. Kwadijk, A.A. Koelmans, Strong sorption of PCBs to nanoplastics, microplastics, carbon nanotubes, and fullerenes, Environmental Science and Technology, 48 (2014) 4869–4876.
[17] M. Zhang, L. Xu, Transport of micro- and nanoplastics in the environment: Trojan-Horse effect for organic contaminants, Critical Reviews in Environmental Science and Technology, (2022).
[18] Ž. Roje, K. Ilić, E. Galić, I. Pavičić, P. Turčić, Z. Stanec, I.V. Vrček, Synergistic effects of parabens and plastic nanoparticles on proliferation of human breast cancer cells, Arh Hig Rada Toksikol, 70 (2019) 310–314.
[19] N. Sun, H. Shi, X. Li, C. Gao, R. Liu, Combined toxicity of micro/nanoplastics loaded with environmental pollutants to organisms and cells: Role, effects, and mechanism, Environment International, 171 (2023) 107711.
[20] R. Trevisan, D. Uzochukwu, R.T. Di Giulio, PAH Sorption to Nanoplastics and the Trojan Horse Effect as Drivers of Mitochondrial Toxicity and PAH Localization in Zebrafish, Front. Environ. Sci., 8 (2020).
[21] J. Zhao, M.H. Stenzel, Entry of nanoparticles into cells: the importance of nanoparticle properties, Polym. Chem., 9 (2018) 259–272.
[22] Y. Ji, Y. Wang, D. Shen, Q. Kang, L. Chen, Mucin corona delays intracellular trafficking and alleviates cytotoxicity of nanoplastic-benzopyrene combined contaminant, Journal of Hazardous Materials, 406 (2021) 124306.
[23] I. Fiorentino, R. Gualtieri, V. Barbato, V. Mollo, S. Braun, A. Angrisani, M. Turano, M. Furia, P.A. Netti, D. Guarnieri, S. Fusco, R. Talevi, Energy independent uptake and release of polystyrene nanoparticles in primary mammalian cell cultures, Experimental Cell Research, 330 (2015) 240–247.
[24] A. Katsumiti, M.P. Losada-Carrillo, M. Barros, M.P. Cajaraville, Polystyrene nanoplastics and microplastics can act as Trojan horse carriers of benzo(a)pyrene to mussel hemocytes in vitro, Sci Rep, 11 (2021) 22396.
[25] S. Yuan, H. Zhang, S. Yuan, Understanding the transformations of nanoplastic onto phospholipid bilayers: Mechanism, microscopic interaction and cytotoxicity assessment, Sci Total Environ, 859 (2023) 160388.
[26] J.-B. Fleury, V.A. Baulin, Microplastics destabilize lipid membranes by mechanical stretching, PNAS, 118 (2021).

https://doi.org/10.26434/chemrxiv-2024-mwgqr **ORCID:** https://orcid.org/0000-0002-4842-828X Content not peer-reviewed by ChemRxiv. **License:** CC BY-NC-ND 4.0

[27] B. Wang, L. Zhang, S.C. Bae, S. Granick, Nanoparticle-induced surface reconstruction of phospholipid membranes, Proc Natl Acad Sci U S A, 105 (2008) 18171–18175.
[28] X. Yong, K. Du, Effects of Shape on Interaction Dynamics of Tetrahedral Nanoplastics and the Cell Membrane, J. Phys. Chem. B, 127 (2023) 1652–1663.
[29] O. Hollóczki, S. Gehrke, Can Nanoplastics Alter Cell Membranes?, Chemphyschem, 21 (2020) 9–12.
[30] D. Bochicchio, E. Panizon, L. Monticelli, G. Rossi, Interaction of hydrophobic polymers with model lipid bilayers, Sci Rep, 7 (2017) 6357.
[31] S. Hong, P.R. Leroueil, E.K. Janus, J.L. Peters, M.-M. Kober, M.T. Islam, B.G. Orr, J.R. Baker, M.M. Banaszak Holl, Interaction of polycationic polymers with supported lipid bilayers and cells: nanoscale hole formation and enhanced membrane permeability, Bioconjug Chem, 17 (2006) 728–734.
[32] S. Qian, V.K. Sharma, L.A. Clifton, Understanding the Structure and Dynamics of Complex Biomembrane Interactions by Neutron Scattering Techniques, Langmuir, 36 (2020) 15189–15211.
[33] J.D. Nickels, S. Chatterjee, C.B. Stanley, S. Qian, X. Cheng, D.A.A. Myles, R.F. Standaert, J.G. Elkins, J. Katsaras, The in vivo structure of biological membranes and evidence for lipid domains, PLOS Biology, 15 (2017) e2002214.
[34] D.K. Rai, S. Qian, W.T. Heller, The Interaction of Melittin with Dimyristoyl Phosphatidylcholine-Dimyristoyl Phosphatidylserine Lipid Bilayer Membranes, Biochimica et Biophysica Acta (BBA) - Biomembranes, 1858 (2016) 2788–2794.
[35] D.K. Rai, S. Qian, Interaction of the Antimicrobial Peptide Aurein 12 and Charged Lipid Bilayer, Scientific Reports, 7 (2017) 3719.
[36] S. Qian, W.T. Heller, Melittin-induced cholesterol reorganization in lipid bilayer membranes, Biochimica et Biophysica Acta (BBA) - Biomembranes, (n.d.).
[37] D.K. Rai, V.K. Sharma, D. Anunciado, H. O'Neill, E. Mamontov, V. Urban, W.T. Heller, S. Qian, Neutron Scattering Studies of the Interplay of Amyloid β Peptide(1–40) and An Anionic Lipid 1,2-dimyristoyl-sn-glycero-3-phosphoglycerol, Sci Rep, 6 (2016) 30983.
[38] B. Chaudhuri, I.G. Muñoz, S. Qian, V.S. Urban, eds., Biological Small Angle Scattering: Techniques, Strategies and Tips, Springer Singapore, 2017.
[39] V.K. Sharma, S. Qian, Effect of an Antimicrobial Peptide on Lateral Segregation of Lipids: A Structure and Dynamics Study by Neutron Scattering, Langmuir, 35 (2019) 4152–4160.
[40] S. Chakraborty, M. Doktorova, T.R. Molugu, F.A. Heberle, H.L. Scott, B. Dzikovski, M. Nagao, L.-R. Stingaciu, R.F. Standaert, F.N. Barrera, J. Katsaras, G. Khelashvili, M.F. Brown, R. Ashkar, How cholesterol stiffens unsaturated lipid membranes, Proceedings of the National Academy of Sciences, 117 (2020) 21896–21905.
[41] S. Qian, P.A. Zolnierczuk, Interaction of a short antimicrobial peptide on charged lipid bilayer: A case study on aurein 12 peptide, BBA Advances, 2 (2022) 100045.
[42] S. Qian, G. Nagy, P. Zolnierczuk, E. Mamontov, R. Standaert, Nonstereotypical Distribution and Effect of Ergosterol in Lipid Membranes, J. Phys. Chem. Lett., 15 (2024) 4745–4752.
[43] M. Törnkvist, G. Larsson, S.-O. Enfors, Protein release and foaming in Escherichia coli cultures grown in minimal medium, Bioprocess Engineering, 15 (1996) 231–237.
[44] E.G. Bligh, W.J. Dyer, A rapid method of total lipid extraction and purification, Can J Biochem Physiol, 37 (1959) 911–917.

https://doi.org/10.26434/chemrxiv-2024-mwgqr **ORCID:** https://orcid.org/0000-0002-4842-828X Content not peer-reviewed by ChemRxiv. **License:** CC BY-NC-ND 4.0

[45] S. Qian, W.T. Heller, Peptide-Induced Asymmetric Distribution of Charged Lipids in a Vesicle Bilayer Revealed by Small-Angle Neutron Scattering, The Journal of Physical Chemistry B, 115 (2011) 9831–9837.
[46] W.T. Heller, M. Cuneo, L. Debeer-Schmitt, C. Do, L. He, L. Heroux, K. Littrell, S.V. Pingali, S. Qian, C. Stanley, V.S. Urban, B. Wu, W. Bras, The suite of small-angle neutron scattering instruments at Oak Ridge National Laboratory, J Appl Cryst, J Appl Crystallogr, 51 (2018) 242–248.
[47] A. Sokolova, A.E. Whitten, L. de Campo, J. Christoforidis, A. Eltobaji, J. Barnes, F. Darmann, A. Berry, Performance and characteristics of the BILBY time-of-flight small-angle neutron scattering instrument, J Appl Cryst, 52 (2019) 1–12.
[48] J. Berghausen, J. Zipfel, P. Lindner, W. Richtering, Influence of Water-Soluble Polymers on the Shear-Induced Structure Formation in Lyotropic Lamellar Phases, J. Phys. Chem. B, 105 (2001) 11081–11088.
[49] B. Hammouda, A new Guinier–Porod model, Journal of Applied Crystallography, 43 (2010) 716–719.
[50] A. Guinier, G. Fournet, Small-angle scattering of X-rays, Wiley, 1955.
[51] M. Ohl, M. Monkenbusch, N. Arend, T. Kozielewski, G. Vehres, C. Tiemann, M. Butzek, H. Soltner, U. Giesen, R. Achten, H. Stelzer, B. Lindenau, A. Budwig, H. Kleines, M. Drochner, P. Kaemmerling, M. Wagener, R. Möller, E.B. Iverson, M. Sharp, et al., The spin-echo spectrometer at the Spallation Neutron Source (SNS), Nuclear Instruments and Methods in Physics Research Section A: Accelerators, Spectrometers, Detectors and Associated Equipment, 696 (2012) 85–99.
[52] P.A. Zolnierczuk, O. Holderer, S. Pasini, T. Kozielewski, L.R. Stingaciu, M. Monkenbusch, Efficient data extraction from neutron time-of-flight spin-echo raw data, J Appl Cryst, 52 (2019) 1022–1034.
[53] A.G. Zilman, R. Granek, Undulations and Dynamic Structure Factor of Membranes, Phys. Rev. Lett., 77 (1996) 4788–4791.
[54] M.C. Watson, F.L.H. Brown, Interpreting Membrane Scattering Experiments at the Mesoscale: The Contribution of Dissipation within the Bilayer, Biophysical Journal, 98 (2010) L9–L11.
[55] M. Nagao, E.G. Kelley, R. Ashkar, R. Bradbury, P.D. Butler, Probing Elastic and Viscous Properties of Phospholipid Bilayers Using Neutron Spin Echo Spectroscopy, J. Phys. Chem. Lett., 8 (2017) 4679–4684.
[56] M.J. Keller, Q. Zhang, S. Qian, B.C. Sanders, H.M. O'Neill, R.L. Hettich, Characterization of the In Vivo Deuteration of Native Phospholipids by Mass Spectrometry Yields Guidelines for Their Regiospecific Customization, Anal. Chem., 96 (2024) 212–219.
[57] O. Glatter, Scattering Methods and their Application in Colloid and Interface Science, 1st Edition, Elsevier, Amsterdam, Netherlands, 2018.
[58] M.-T. Lee, F.-Y. Chen, H.W. Huang, Energetics of Pore Formation Induced by Membrane Active Peptides†, Biochemistry, 43 (2004) 3590–3599.
[59] R.H. Ottewill, A. Parentich, R.A. Richardson, Osmotic pressure measurements on strongly interacting polymer colloid dispersions, Colloids and Surfaces A: Physicochemical and Engineering Aspects, 161 (2000) 231–242.

https://doi.org/10.26434/chemrxiv-2024-mwgqr **ORCID:** https://orcid.org/0000-0002-4842-828X Content not peer-reviewed by ChemRxiv. **License:** CC BY-NC-ND 4.0